Inorganic Chemistry

Article

pubs.acs.org/IC

Electrochemical Evidence of Intramolecular Electronic Communication in Zr and Hf Phthalocyanines Bearing Ferrocene-Containing β-Diketonato Axial Ligands: Structure of [PcHf(FcCOCHCOC$_6$H$_5$)$_2$]

Blenerhassitt E. Buitendach,[†] Anna Gągor,[‡] and Jannie C. Swarts*,[†]

[†]Department of Chemistry, University of the Free State, P.O. Box 339, Bloemfontein, 9300, Republic of South Africa

[‡]Institute of Low Temperature and Structure Research, PAS, Okólna 2, 50-950 Wroclaw, Poland

Supporting Information

ABSTRACT: The series of zirconium(IV) and hafnium(IV) phthalocyanine complexes [PcM(FcCOCHCOR)$_2$] (Pc = phthalocyaninato; M = Zr; R = CF_3 (**1**), CH_3 (**2**), C_6H_5 (**3**), Fc ($(C_5H_5)Fe(C_5H_4)$, **4**), as well as M = Hf ; R = CF_3 (**5**), CH_3 (**6**), C_6H_5 (**7**), and Fc (**8**)) were synthesized. A single-crystal X-ray diffraction analysis of the structure of [PcHf(FcCOCHCOC$_6$H$_5$)$_2$], **7** (Z = 2, space group $P\bar{1}$), showed the two axial β-diketonato ligands were orientated in such a way that the ferrocenyl groups were positioned diagonally opposite each other. From the structural determination of **7** it was clear that these complexes have a distorted D_{4h} symmetry at the coordination site of the metal centers, which explains a splitting of the UV−vis Q band into Q_x and Q_y components with $3 \leq \Delta\lambda_{max,Q} \leq 10$ nm. Cyclic and square wave voltammetric studies in CH_2Cl_2/[N(^{n}Bu)$_4$][B(C_6F_5)$_4$] allowed observation of at least three phthalocyaninato macrocycle-based redox couples as well as all (i.e., two or four) well-resolved ferrocenyl couples in **1**−**8**. For M = Zr and R = Fc, formal reduction potentials of the four ferrocenyl groups were found to be $E^{\circ\prime}$ = 296, 386, 538, and 687 mV versus free ferrocene. Spectroelectrochemical evidence, UV−vis Q-band maximum wavelengths, and HOMO−LUMO energy gaps as expressed by $\Delta E^{\circ\prime}{}_{I-III} = \Delta E^{\circ\prime}{}_{wave\ I} - \Delta E^{\circ\prime}{}_{wave\ III}$ were mutually consistent, indicating that the first phthalocyaninato ring-based oxidation occurs before ferrocenyl oxidations take place. The potential for each redox process was found to be dependent on the sum of β-diketonato R-group group electronegativities, $\Sigma\chi_R$. Mathematical relationships for the dependency of $E^{\circ\prime}$ on $\Sigma\chi_R$ for all four observed ring-based redox processes as well as for the ferrocenyl-based redox processes were determined. This allowed prediction of potentials for redox processes that fall outside the workable potential window of the solvent. No significant differences were found between the corresponding redox potentials of zirconium and hafnium analogues bearing the same axial ligands.

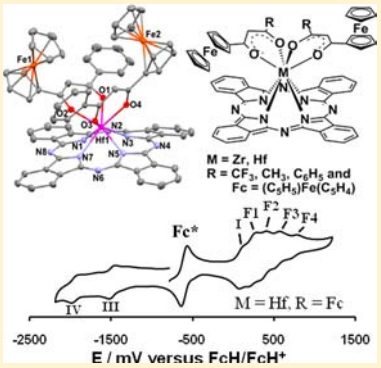

INTRODUCTION

The high stability and exceptional photophysical,[1] photochemical,[2] electrochemical,[3] and coordination properties[4] of phthalocyanines caused them to be studied in diverse high technological areas such as semiconductor devices,[5] liquid crystals,[6] sensors,[7] catalysts,[8] nonlinear optics,[9] photovoltaic solar cells,[10] antiviral research,[11] and photodynamic cancer therapy.[12] Computational studies assisted much in the current understanding of unusual axial binding modes of these porphyrin derivatives.[13] The low solubility of many metallophthalocyanines is the result of aggregation in solution. Aggregation can substantially impede desired physical and chemical properties of phthalocyanines such as photoactivity in organic photovoltaics, or it can impair photodynamic activity in diseased cell tissue when these compounds act as photosensitizers in photodynamic therapy. Introduction of axial ligands to the central metal atom of many metallophthalocyanine complexes is known to influence the properties of the metallophthalocyanines to a large degree, and it can decrease aggregation substantially.[14]

The high stability of di(chloro)zirconium and -hafnium phthalocyanine complexes allows for synthesis of new compounds by direct exchange of the chloride ligand with other ligands.[15] Tomachynski and co-workers synthesized zirconium and hafnium phthalocyanine complexes of the type PcM(β-diketonato)$_2$, where M = Zr^{IV} and Hf^{IV} and β-diketonato = RCOCHCOR′, where R and R′ included CH_3, CF_3, $C(CH_3)_3$, and C_6H_5.[16] They found that the compounds do not aggregate in organic solvents at lower concentrations than 10^{-5} mol dm^{-3}. All Tomachynski β-diketonato phthalocyanine complexes were crystalline substances that dissolve in most organic solvents (benzene, toluene, chloroform, and others). In contrast, the dichloro complexes were found to have much lower solubilities. The electrochemistry of all these complexes was also studied by the Tomachynski−Kadish collaboration.[16c] It was found that all compounds exhibited at least two ring-based oxidations and two ring-based reduction

Received: December 12, 2012
Published: August 23, 2013

   dx.doi.org/10.1021/ic302730v | Inorg. Chem. 2013, 52, 10245−10257

processes and that Zr and Hf were redox silent. Unusually though, complexes with R and R′ being CF_3 and C_6H_5 exhibited four ring-based reduction processes and three oxidations within the solvent (CH_2Cl_2) potential window. None of these complexes had any redox-active substituents like a ferrocenyl group either on the phthalocyaninato ring or on the axial β-diketonato ligands.

The ferrocenyl group is frequently a component of new organometallic complexes and functional materials due to its good stability and ease by which ferrocene can be chemically modified.[17] Due to the electrochemical reversible behavior of the iron(II/III) couple, ferrocene derivatives are frequently the subject of electrochemical studies.[18] The electron-donating properties of the ferrocenyl group are known to enhance the rate of oxidative addition reactions.[19] Ferrocene derivatives have also been studied in asymmetric catalysis,[20] as high burning rate catalyst in solid propellants,[21] as nonlinear optics,[22] as donors in energy transfer processes,[23] and as anticancer drugs.[24] Ferrocene-containing β-diketones of the type $FcCOCH_2COR$ (with R = CF_3, CH_3 C_6H_5, and Fc) have been synthesized and characterized[25] as well as tested for cytotoxic activity.[24b] The trifluoro-containing β-diketone ($FcCOCH_2COCF_3$) was the most cytotoxic.

In this study we report the synthesis of new ferrocene-containing β-diketonato complexes of zirconium and hafnium phthalocyanines [$PcM(FcCOCHCOR)_2$] (M = Zr and R = CF_3 (**1**), CH_3 (**2**), C_6H_5 (**3**), and Fc (**4**) as well as M = Hf and R = CF_3, **5**; CH_3, **6**; C_6H_5, **7** and Fc, **8**), characterize them structurally, and highlight intramolecular communication between ferrocenyl groups from results of an electrochemical study in the presence of $[N(^nBu)_4][B(C_6F_5)_4]$ as supporting electrolyte. Successive ferrocenyl formal redox potentials are shown to be a function of group electronegativity, χ_R.[26]

RESULTS AND DISCUSSION

Synthesis. Dichloro(phthalocyaninato)zirconium(IV) ($PcZrCl_2$), **9**, and dichloro(phthalocyaninato)hafnium(IV) ($PcHfCl_2$), **10**, were synthesized[16a] by cyclotetramerization of phthalonitrile in the presence of the corresponding metal tetrachloride, Scheme 1. The presence of 2-methylnaphthalene as chloride radical scavenger prevented chlorination of the phthalocyanine ring,[16a] while the high-boiling solvent 1,2,4-trichlorobenzene was used to suppress formation of PcM^{IV} oxides such as Pc(Zr/Hf)O or Pc(Zr/Hf)(OH).[16a] Phthalocyaninato β-diketonato complexes **1**−**8** were then obtained by reacting dichlorophthalocyanines **9** and **10** with β-diketones **11**−**14**, Scheme 1, to liberate [$PcM(FcCOCHCOR)_2$] complexes **1**−**8** in 14−71% yield, Table 1. The previously reported[16a,c] actylacetonato derivatives [$PcZr(CH_3COCHCOCH_3)_2$], **15**, and [$PcHf(CH_3COCHCOCH_3)_2$], **16**, were also prepared to compare our results of the present new ferrocene-containing complexes with those of the Tomachynski complexes.[16a,c] All dark blue-purple β-diketonato-phthalocyanato complexes were noticeably more soluble in common organic solvents such as dichloromethane or tetrahydrofuran than their dichloro precursors **9** and **10**.

Crystal Structure of [$PcHf(FcCOCHCOC_6H_5)_2$], 7. [$PcHf(FcCOCHCOC_6H_5)_2$] crystallized by slow evaporation−diffusion using THF as primary solvent and *n*-hexane as secondary solvent into a triclinic crystal system with *P*-1 space group. Crystal data are shown in Table 2, and different views of the molecular structure of **7**, highlighting atom labeling, are shown in Figure 1. Selected bond distances (Angstroms) and bond angles (degrees) are summarized in the caption of Figure 1.

Scheme 1. Synthetic Route toward [$PcM(FcCOCHCOR)_2$] Complexes 1−8

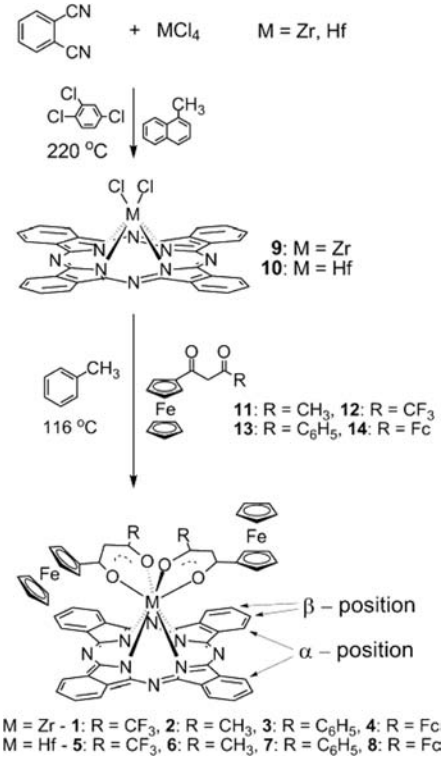

The structure of **7** highlights intramolecular through-bond communication of one molecular fragment of **7** with another. However, before discussing the structure of **7**, it is useful to note that typical single-bond C−C lengths range from 1.38 (sp−sp, —C≡C—C≡C—) to 1.53 Å (sp^3−sp^3, —C—C—), while double bonds range from 1.28 (sp−sp ═C═C═) to 1.32 Å (sp^2−sp^2 —C═C—).[27] C−C bonds in compounds that are delocalized are expected to have distances that lie between the 1.48 Å of an sp^2−sp^2 ═C—C═ single bond and the 1.32 Å of an sp^2−sp^2 —C═C— double bond.[28]

The two β-diketonato ligands are coordinated in such a way that the ferrocenyl moieties are diagonally on opposite sides of the central hafnium atom. We label this geometry as the T isomer. Both ferrocenyl groups project up and away from the phthalocyanine macrocycle. All C−C bonds in the β-diketonato ligand of complex **7**, except the C-phenyl bonds C(40)−C(41) = 1.535(10) Å and C(59)−C(60) = 1.505(8) Å, have lengths that are between 1.32 and 1.48 Å. Thus, C−C bonds in the β-diketonato backbones have delocalized character and in principle should be capable of conveying any electron-withdrawing or -donating effects from other parts of the β-diketonato ligand to and from the ferrocenyl group. The relatively small differences between the two C−C bond lengths adjacent to the methine carbon atoms C(39) and C(58) in the (O)C−CH−C(O) backbone of the β-diketonato ligands are 0.011 and 0.026 Å, respectively. Thus, both β-diketonato fragments are weakly asymmetric, implying the group electronegativity of the pendent ferrocenyl (χ_{Fc} = 1.87) and phenyl groups (χ_{Ph}= 2.21) differs just enough to lead to weakly asymmetric β-diketonato ligands. The β-diketonato backbone

dx.doi.org/10.1021/ic302730v | Inorg. Chem. 2013, 52, 10245−10257

Table 1. Yields, Q-Band Absorption Maxima of Q_x and Q_y Components in THF (ca. 5 μmol dm^{-3} solutions), $\Delta\lambda_{max}$, and Possible $\Delta E^{o\prime}$ Values for 1−8, 15, and 16

no. (M; R^1; R^2)[a]	yield/%	$\lambda_{max,Qx}$/nm (ε_{Qx}); $\lambda_{max,Qy}$/nm (ε_{Qy}/dm^3 mol^{-1}cm^{-1})[b]	$\Delta\lambda_{max}$/nm[c]	$\Delta E^{o\prime}_{I-III}$/V[d]	$\Delta E^{o\prime}_{F1-III}$/V[d]	$\Delta E^{o\prime}_{F2-III}$/V[d]
1, Zr; Fc; CF_3	66	681 (159 900); 689 (159 300)	8	1.601	1.792	1.959
2, Zr; Fc; CH_3	14	681 (161 200); 687 (159 000)	6	1.593	1.714	1.908
3, Zr; Fc; Ph	41	683 (173 200); 686 (172 700)	3	1.602	1.730	1.905
4, Zr; Fc; Fc	33	683 (141 500); 686 (139 200)	3	1.603	1.777	1.867
5, Hf; Fc; CF_3	71	679 (157 500); 688 (156 100)	9	1.611	1.802	1.964
6, Hf; Fc; CH_3	56	679 (159 900); 687 (156 100)	8	1.598	1.708	1.894
7, Hf; Fc; Ph	53	682 (166 400); 687 (165 800)	5	1.598	1.715	1.881
8, Hf; Fc; Fc	61	682 (166 900); 687 (164 000)	5	1.610	1724	1.856
15, Zr; CH_3; CH_3	32	677 (98 800); 687 (104 900)	10	1.598		
16, Hf; CH_3; CH_3	38	676 (133 900); 686 (142 200)	10	1.589		

[a] R^1 and R^2 are pendant groups in β-diketonato ligands $(R^1COCHCOR^2)^-$. [b] Values in brackets are the extinction coefficients (ε) of the Q_x and Q_y components of the Q band. [c] $\Delta\lambda_{max}$ = (λ_{max} for Q_y) − (λ_{max} for Q_x). [d] $E^{o\prime}$ for waves I, III, F1, and F2 may be found in Table 2; $\Delta E^{o\prime}_{I-III} = E^{o\prime}_{I} - E^{o\prime}_{III}$; $\Delta E^{o\prime}_{F1-III} = E^{o\prime}_{F1} - E^{o\prime}_{III}$; $\Delta E^{o\prime}_{F2-III} = E^{o\prime}_{F2} - E^{o\prime}_{III}$.

Table 2. Crystal Data, Structure, and Refinement Details for $PcHf(FcCOCHCOPh)_2$, 7

empirical formula	$C_{70}H_{46}Fe_2HfN_8O_4$	abs coeff/mm^{-1}	2.47
mol wt	1353.34	θ range for data colln/deg	2.91−25.68
cryst size/mm^3	0.22 × 0.13 × 0.07	index ranges	$-15 \le h \le 15$, $-17 \le k \le 17$, $-19 \le l \le 19$
temp./K	295	no. of reflns collected	30 011
wavelength/Å	0.71073	no. of independent reflns	10 398 [R(int) = 0.106]
cryst syst	triclinic	completeness to θ = 25.68°	99.8%
space group	P-1	max and min transmission	1.00000 and 0.93631
unit cell dimensions/Å	a = 12.8711(7)	refinement method	full-matrix least-squares on F^2
	b = 14.3680(7)	data/restraints/params	10 398/0/766
	c = 16.4049(9)	goodness-of-fit on F^2	0.846
vol./Å^3	2743.2 (3)	final R indices [$I > 2\sigma(I)$]	R1 = 0.0540, wR2 = 0.0815
Z	2	R indices (all data)	R1 = 0.1580, wR2 = 0.0650
density (calcd)/Mg m^{-3}	1.638	absolute structure parameter	0.035(17)
F(000)	1360	largest diff. peak and hole/e Å^{-3}	0.84 and −0.57

C−C bonds closest to the more electron-withdrawing phenyl group in the (O)C−CH−C(O) backbone are the shortest.

The cyclopentadienyl rings of both ferrocenyl groups are in the staggered conformation. The deviation from the eclipsed conformation for Fc1 and Fc2, as measured with the dihedral angles C(47)−centroid$_{Cp\ ring}$−centroid$_{subst\ Cp\ ring}$−C(33) and C(66)−centroid$_{Cp\ ring}$−centroid$_{subst\ Cp\ ring}$−C(52) were found to be 14.29° and 23.35°, respectively. The distances between the cyclopentadienyl rings for ferrocenyl groups Fc1 and Fc2 were determined at 3.285 and 3.289 Å, respectively. It was found that the cyclopentadienyl rings of both ferrocenyl groups were nearly parallel, with the dihedral angle between cyclopentadienyl planes for Fc1 and Fc2 at 1.68° and 0.88°, respectively. The average C−C bond distances in the ferrocenyl groups are 1.387 Å for the unsubstituted cyclopentadienyl rings and 1.409 Å for substituted cyclopentadienyl rings. The longest bond is C(52)−C(53), 1.428(8) Å, while the shortest bond is C(47)−C(51), 1.363(10) Å. Bond angles in the unsubstituted and substituted cyclopentadienyl rings averaged 108°, the ideal theoretical value. The largest deviations from the average values were C(35)−C(36)−C(37) (+1.00°) on a substituted Cp ring and C(66)−C(70)−C(69) (+2.96°) on an unsubstituted Cp ring.

Unconjugated C═O bond lengths in β-diketones are typically 1.206 Å long, while single C−O bond lengths are 1.300 Å.[29] For 7, all C−O bonds lengths fall within these extremes. The shortest is C(59)−O(3) with a length of 1.253(7) Å, and the longest is C(38)−O(2) = 1.285(7) Å. The difference between the longest and the shortest C−O bonds in 7 is 0.032 Å, while the difference between unconjugated C═O and C−O bonds in β-diketones is 0.094 Å.[29] It is clear that the C−O bonds encountered in 7 are much longer than typical C═O bonds and meaningfully shorter than C−O bonds and thus also indicative of significant delocalized character in both β-diketonato fragments. Delocalized bonding thus occurs throughout the two axial β-diketonato ligands and electron-withdrawing or -donating effects from electrochemically generated charged ferrocenium (Fe^{3+}, χ_{Fc+} = 2.82), neutral ferrocenyl (Fe^{2+}, χ_{Fc} = 1.87), and any R-β-diketonato group may therefore be transmitted from the β-diketonato ligand to a metal coordinated to it.

The remaining question to be answered to understand how a substituent on one of the β-diketonato ligands of 7 in principle can transmit any electronic effects it may have to another β-diketonato ligand or the phthalocyanine macrocycle is an understanding of how these effects may cross the hafnium core of 7.

The Hf(1) atom in $[PcHf(FcCOCHCOC_6H_5)_2]$, 7, has a slightly distorted square antiprismatic coordination sphere. The bond angles at this atom vary in the comparatively narrow ranges of 71.2(2)−80.1(2)°, 109.6(2)−118.7(2)°, and 139.6(2)−143.5(2)°. The Hf(1)−O bond lengths average 2.155 Å with a range of 2.144(4)−2.162(4) Å, while the Hf(1)−N bond lengths average 2.282 Å with a range of 2.276(5)−2.291(5) Å. The differences in the average Hf(1)−N distances in particular results in a narrow splitting of the Q band of complex 7's UV−vis spectrum ($\Delta\lambda_{max}$ = 5 nm) as it contributes in breaking the D_{4h} symmetry of the phthalocyaninato fragment of the molecule.

The largest deviations from the Hf−O bond length average of 2.155 Å is 0.011 Å for Hf−O(3), which has a bond length of

dx.doi.org/10.1021/ic302730v | Inorg. Chem. 2013, 52, 10245−10257

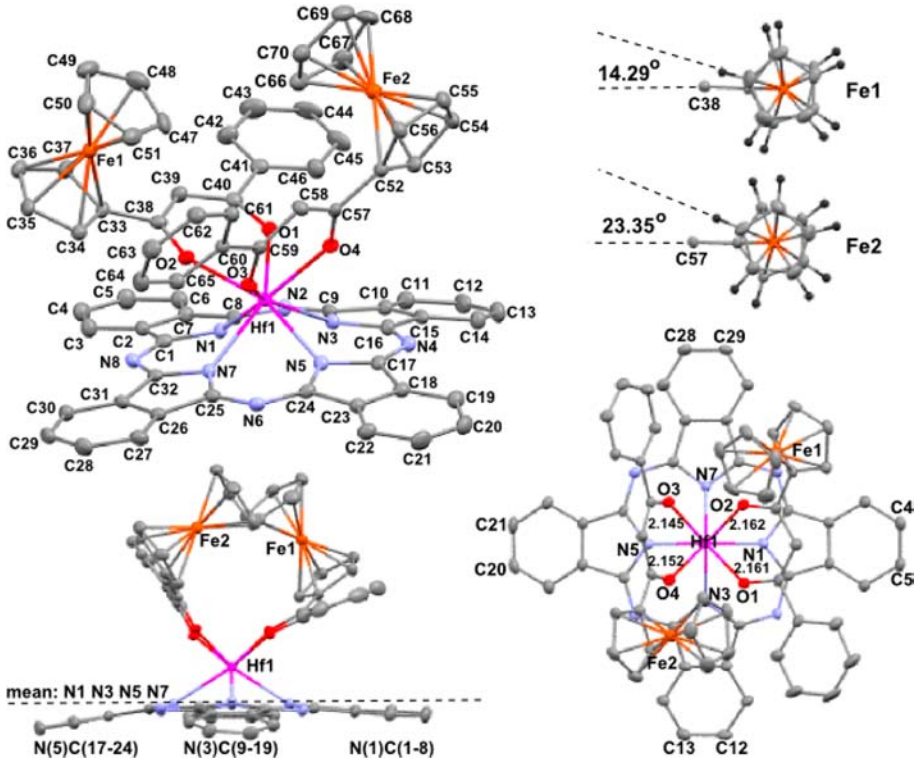

Figure 1. Molecular structure of $[PcHf(FcCOCHCOC_6H_5)_2]$, **7**, showing atom labeling (top left). Bottom right view shows a top-down perspective of **7** highlighting the position of the ferrocenyl moieties with respect to each other. Bottom left view shows a side-on perspective highlighting the distortion of the phthalocyanine macrocycle from planarity. Hydrogen atoms are not shown for clarity. Staggered conformation of the two ferrocenyl moieties is shown in the top right view. Selected bond distances (Angstroms) and angles (degrees) are as follows (see Supporting Information for complete list of data): Hf–N(1) 2.283(5), Hf–N(3) 2.276(5), Hf–N(5) 2.291(5), Hf–N(7) 2.279(5), N(1)–C(1) 1.381(7), C(1)–C(2) 1.439(8), C(2)–C(3) 1.395(8), C(2)–C(7) 1.369(8), C(3)–C(4) 1.382(8), C(4)–C(5) 1.378(9), C(6)–C(7) 1.388(8), C(7)–C(8) 1.440(8), N(1)–C(8) 1.371(7), avg. C–N(1,3,5,7) 1.381, avg. C–N(2,4,6,8) 1.322, C(33)–C(38) 1.475(9), C(38)–C(39) 1.396(8), C(39)–C(40) 1.385(8), C(40)–C(41) 1.535(10), C(40)–O(1) 1.277(7), C(38)–O(2) 1.285(7), Hf–O(1) 2.161(5), Hf–O(2) 2.162(4), Hf–O(3) 2.144(4), Hf–O(4) 2.151(5), avg. C_p C–C 1.398 (C(47)–C(51) 1.363(10) to C(52)–C(53) 1.428(8)); C(38)–C(39)–C(40) 120.2(7), O(1)–C(40)–C(39) 124.7(8), O(2)–C(38)–C(39) 124.0(7), O(1)–C(40)–C(41) 113.2(7), O(2)–C(38)–C(33) 115.7(7).

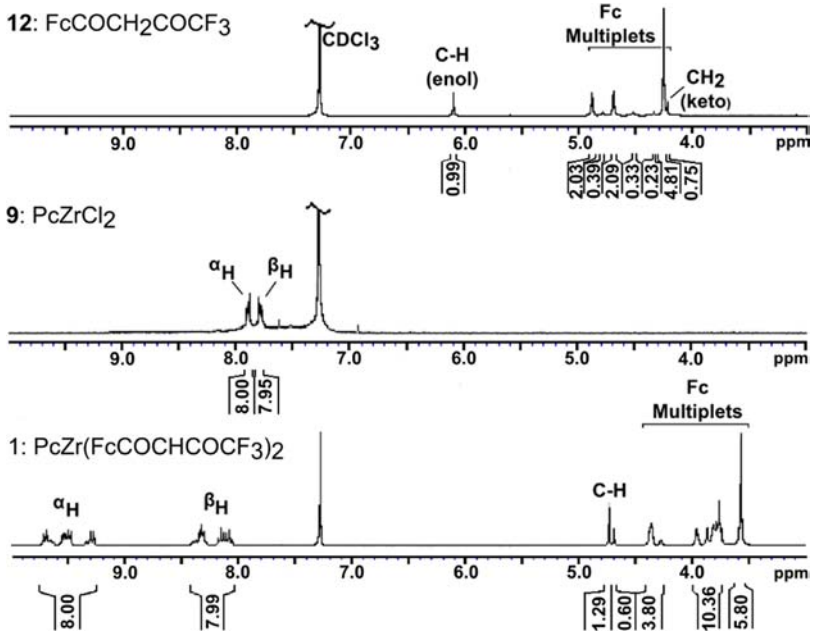

Figure 2. ^1H NMR spectra in $CDCl_3$ of **2**, **9**, and **12**.

2.144(4). The difference between the largest (Hf–O(2) = 2.162(4) Å) and the smallest (Hf–O(3)) Hf–O bond lengths is 0.018 Å. The largest deviations from the Hf–N bond average of 2.282 Å is 0.009 Å for Hf–N(5) = 2.291(5) Å. The

dx.doi.org/10.1021/ic302730v | Inorg. Chem. 2013, 52, 10245–10257

difference between the longest (Hf−N(5)) and the shortest (Hf−N(3) = 2.276(5) Å) Hf−N bond lengths is 0.015 Å. These average Hf−N and Hf−O bond lengths are longer than typical Hf−OR (1.925 Å) bond lengths or shorter than Hf−NR_3 (2.418 Å) bond lengths.[30] In particular, the short Hf−N bonds of **7** suggest through-bond electronic communication will be possible through the Hf core of **7**. The C−C bond lengths of the aromatic phthalocyanine macrocycle fall within the range 1.350(9)−1.455(9) Å. The shortest phthalocyanine C−C bond is 1.350(9) Å for C(19)−C(20)n while C(25)−C(26) = 1.455(9) Å is the longest. The average phthalocyaninato C−C bond length is 1.398 Å. Thus, it is expected that the delocalized phthalocyanine macrocycle C−C bonds will transmit any electron-withdrawing or -donating electronic effects from axial ligands through its plane after it crossed the Hf center.

The central N(1−8)C(1)C(8)C(9)C(16)C(17)C(24)-C(25)C(32) macrocycle of the phthalocyanine ligand is not exactly planar (deviations from the least-squares plane exceed 0.15 Å) and has the appearance of a much flattened crown. The Hf(1) atom is 1.338(3) Å above this least-squares plane. The dihedral angles between the N(1)N(3)N(5)N(7) plane and planar bicyclic systems N(1)C(1−8), N(3)C(9−16), N(5)C(17−24), and N(7)C(25−32) are 5.4°, 14.0°, 10.5°, and 3.7°, respectively. The six-membered pseudoaromatic HfO_2C_3 heterocyclic cores formed by the Hf and *β*-diketonato ligands in **7** are also not planar, with dihedral angles between the O(1)Hf(1)O(2) plane and the planar *β*-diketonato ligand O(1)C(38−40)O(2) at 15.92° and between the O(3)Hf(1)-O(4) plane and the planar *β*-diketonato ligand O(3)C(57−59)O(4) at 18.93°. These large dihedral angle distortions from 0° are significant in explaining the split Q bands discussed below.

Thus, in summary, the crystal structure of **7** suggests good electronic communication between the different ferrocenyl moieties and electronic interaction with the phthalocyanine macrocycle is possible due to the delocalized nature of the C−C backbone in the *β*-diketonato and phthalocyanine fragments and the short Hf−N bonds. The capability of **7** to transmit electronic effects from one end of the molecule to the other was studied and quantified with the mathematical formulas in the electrochemical section of this study.

^{1}H NMR Spectroscopy of 1−8, 15, and 16. Figure 2 shows the ^{1}H NMR spectra in $CDCl_3$ of [PcZr-$(FcCOCHCOCF_3)_2$], **1**, together with the spectrum of the free *β*-diketone $FcCOCH_2COCF_3$, **12**, and the dichlorozirconium(IV) phthalocyanine complex **9**. The aromatic signals of the eight $^{\alpha}$H and $^{\beta}$H protons of **9** shifted downfield upon complexation with the two *β*-diketonato ligands from 7.92−7.77 to 9.75−8.05 ppm for PcZr-$(FcCOCHCOCF_3)_2$, **1**. The coordinated *β*-diketonato methine hydrogens of **1** shifted upfield from 6.11 ppm for the enol form of the free ligand **12** to 4.72 ppm for coordinated *β*-diketonate ligands of **1**. The large downfield shifts of the $^{\alpha}$H and $^{\beta}$H proton signals are considered to be the result of distortion of the NMR's magnetic field by the combined bulk of the phthalocyanine ring and *β*-diketonato ligands probably because of ring current effects. A similar downfield shift of the benzylic proton peak positions of 3,6-di(octadecyl)phthalonitrile at 2.85 ppm was observed after cyclization to phthalocyanines, where the same CH_2 signals resonate at 4.75 ppm.[31] Like **7**, from NMR evidence, complex **1** is clearly not symmetrical because two methane (CH) ^{1}H NMR signals are observed at 4.7 ppm. This means it possesses two geometrically inequivalent *β*-diketonato ligands. We conclude from the inequivalent methine protons in the ^{1}H NMR spectra of **1**−**8** and also the single-crystal X-ray structure determination of **7** that complexes **1**−**8** do not possess true D_{4h} symmetry as many other metalated phthalocyanines have.

In addition, the complexity of both ferrocenyl signals (normally just two triplets and one singlet are expected in the region 4−5 ppm[25]) and the $^{\alpha}$H and $^{\beta}$H proton signals of **1**−**8** over that observed for **9** and **10** is consistent with the *β*-diketonato ligands being involved in dynamic equilibriums involving more than just one isomer in solution upon binding to the Hf or Zr metallic centrums. In the electrochemical section below, evidence will also be presented that supports the existence of more than one isomer in solution. This contrasts the apparent inertness of a single isomer in the solid state toward isomerization as observed crystallographically for **7**, as the structure of **7** was only solved several months after isolation of the crystallographic quality crystals.

UV−vis Spectroscopy. The lack of "true" D_{4h} symmetry has an effect on the electronic spectra of **1**−**8**. Metal-free phthalocyanines have D_{2h} symmetry which gives rise to two Q-band maxima, Q_x and Q_y, in the region 620−700 nm.[31] The exact peak position depends on the substitution pattern on the *α* and *β* positions: $\Delta\lambda = \lambda_{max,Qx} - \lambda_{max,Qy} = 31$ nm, for example, for octa *α*-alkylated metal-free phthalocyanines (i.e., alkylation in the nonperipheral *α*-positions). In contrast, metalated phthalocyanines normally have D_{4h} symmetry with degeneration of the lowest energy singlet state.[31] As result, the Q_x and Q_y bands of the metal-free phthalocyanines coalesce into a single strong Q-band absorption with λ_{max} close to 700 nm.[31] From the ^{1}H NMR spectra of **1**−**8** and structural determination of **7** it is clear that D_{4h} symmetry is not quite achieved in **1**−**8**, and upon inspection of the absorption spectra of **1**−**8** in THF, Q_x and Q_y Figure 3, it was noted that the Q bands are actually

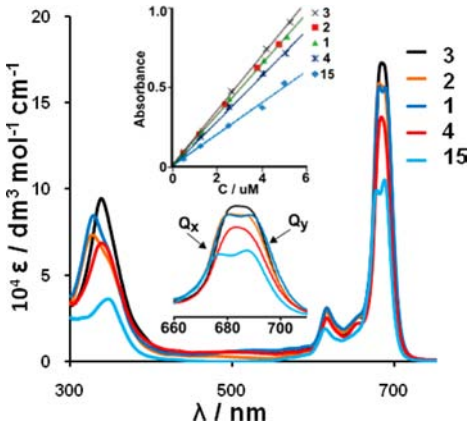

Figure 3. UV−vis spectra of zirconium complexes **1**−**4** and **15** in THF, recorded at concentrations of 5 *μ*mol dm^{-3}. Hafnium analogues **5**−**8** and **16** gave essentially identical spectra (see Supporting Information). (Insert) Complexes followed the Beer−Lambert law till at least 5 *μ*M.

comprised of two closely overlapping separate peaks. λ_{max} values are summarized in Table 1. $PcM(CH_3COCHCOCH_3)_2$ derivatives **15** an **16** have the largest $\Delta\lambda_{max} = 10$ nm peak gap, but this value is considerably smaller than the 31 nm $\Delta\lambda_{max}$ value found in metal-free phthalocyanines.[31] We conclude that the degeneracy of the lowest energy phthalocyaninato singlet

dx.doi.org/10.1021/ic302730v | Inorg. Chem. 2013, 52, 10245−10257

Table 3. Cyclic Voltammetry Data of 0.5 mmol dm^{-3} Solutions of 1−8, 15, and 16 in CH_2Cl_2 Containing 0.2 mol dm^{-3} $[N(^nBu)_4][B(C_6F_5)_4]$ as Supporting Electrolyte at 20 °C[a]

wave[b]	E_{pa}/mV	ΔE_p/mV	$E^{\circ\prime}$/mV	i_{pa}/μA	i_{pc}/i_{pa}
PcZr(FcCOCHCOCF$_3$)$_2$, **1**; *(PcHf(FcCOCHCOCF$_3$)$_2$, **5**)*[f]					
V_a	−2414 *(−2372)*[c]	230 *(221)*	−2299 *(−2262)*	5.63 *(3.75)*[d]	0.65 *(0.55)*[e]
IV_a	−1830 *(−1840)*[c]	94 *(101)*	−1783 *(−1790)*	5.71 *(4.17)*[d]	0.50 *(0.40)*[e,g]
III_a	−1402 *(−1406)*[c]	74 *(64)*	−1365 *(1374)*	6.29 *(5.42)*[d]	0.54 *(0.38)*[e,g]
I	270 *(270)*	84 *(83)*	228 *(229)*	5.46 *(4.48)*	0.92 *(0.93)*
F1	460 *(461)*	78 *(72)*	421 *(425)*	5.77 *(4.42)*	0.98 *(0.95)*
F2	632 *(631)*	84 *(86)*	590 *(588)*	5.21 *(4.22)*	1.03 *(1.05)*
PcZr(FcCOCHCOCH$_3$)$_2$, **2**; *(PcHf(FcCOCHCOCH$_3$)$_2$, **6**)*					
IV_a	−1951 *(−1933)*[c]	90 *(80)*	−1906 *(−1893)*	3.64 *(2.68)*[d]	0.60 *(0.53)*[e]
III_a	−1497 *(−1489)*[c]	74 *(67)*	−1460 *(−1456)*	5.09 *(3.04)*[d]	0.72 *(0.70)*[e,g]
I	167 *(164)*	82 *(69)*	126 *(130)*	4.51 *(2.54)*	1.02 *(1.00)*
F1	299 *(288)*	92 *(71)*	253 *(253)*	4.62 *(2.67)*	0.93 *(0.95)*
F2	483 *(474)*	78 *(67)*	444 *(441)*	4.73 *(2.48)*	0.93 *(1.08)*
II	1257 *(1265)*	72 *(78)*	1221 *(1226)*	3.19 *(2.35)*	0.76 *(0.92)*
PcZr(FcCOCHCOPh)$_2$, **3**; *(PcHf(FcCOCHCOPh)$_2$, **7**)*					
IV_a	−1947 *(−1915)*[c]	70 *(74)*	−1912 *(−1878)*	2.56 *(4.64)*[d]	0.88 *(0.93)*[e]
III_a	−1501 *(−1492)*[c]	68 *(69)*	−1467 *(−1458)*	4.19 *(5.00)*[d]	0.92 *(0.92)*[e,g]
I	161 *(167)*	68 *(69)*	127 *(133)*	4.68 *(4.49)*	0.92 *(0.95)*
F1	299 *(291)*	72 *(68)*	263 *(257)*	4.30 *(4.38)*	0.91 *(1.03)*
F2	485 *(474)*	100 *(103)*	435 *(423)*	4.68 *(4.27)*	0.92 *(0.95)*
II	1265 *(1267)*	76 *(75)*	1227 *(1230)*	3.16 *(4.16)*	0.92 *(0.81)*
PcZr(FcCOCHCOFc)$_2$, **4**; *(PcHf(FcCOCHCOFc)$_2$, **8**)*[f]					
IV_a	−1955 *(−1987)*[c]	68 *(72)*	−1921 *(−1951)*	0.91 *(1.21)*[d]	0.61 *(0.67)*[e]
III_a	−1513 *(−1526)*[c]	64 *(79)*	−1481 *(−1487)*	0.73 *(1.76)*[d]	0.60 *(0.89)*[e,g]
I	157 *(139)*	84 *(65)*	115 *(107)*	3.15 *(1.46)*	0.96 *(0.95)*
F1	337 *(283)*	82 *(98)*	296 *(234)*	2.70 *(1.49)*	0.96 *(0.89)*
F2	423 *(406)*	68 *(69)*	389 *(372)*	2.81 *(1.52)*	1.08 *(1.04)*
F3	571 *(568)*	62 *(67)*	540 *(535)*	2.13 *(1.46)*	1.05 *(1.00)*
F4	719 *(780)*	62 *(71)*	688 *(745)*	2.19 *(1.14)*	1.02 *(0.94)*
PcZr(CH$_3$COCHCOCH$_3$)$_2$, **15**; *(PcHf(CH$_3$COCHCOCH$_3$)$_2$, **16**)*					
IV_a	−1917 *(−1899)*[c]	76 *(107)*	−1879 *(−1845)*	4.36 *(5.45)*[d]	0.83 *(0.67)*[e]
III_a	−1450 *(−1439)*[c]	69 *(78)*	−1416 *(−1400)*	5.27 *(6.36)*[d]	0.79 *(0.80)*[e,g]
I	215 *(224)*	72 *(77)*	179 *(185)*	4.44 *(5.38)*	0.91 *(0.98)*
II	950 *(958)*	131 *(112)*	885 *(902)*	4.51 *(5.66)*	0.63 *(0.58)*

[a]Values given in italics and parentheses are those of the Hf derivatives. [b]Ring-based redox processes are labeled in Roman numerals; ferrocene-based redox processes are labeled with precursor "F". [c]E_{pc} values are given. [d]i_{pc} values are given. [e]i_{pa}/i_{pc}values are given. [f]Complexes **1**, **4**, **5**, and **8** showed no wave II within the potential window CH_2Cl_2 allows. [g]Upon changing the switching potential such that wave IV is eliminated, current ratios for wave III approach unity. Wave IV current ratios came much closer to 1 if wave V is excluded from the CV experiment, but unity was never achieved.

state of **1**−**8** and also the acac complexes **15** and **16** is partially lifted in these complexes but not to the same extent as that observed in metal-free phthalocyanines. The ferrocene-free complexes studied by the Tomachynski−Kadish collaboration[16c] showed a similar Q-band splitting as our ferrocene-containing complexes did, but no explanation was provided for the observed splitting. In contrast, the chloro complexes **9** and **10** do not show Q-band splitting which indicates that true D_{4h} symmetry was achieved (see Supporting Information). Since β-diketonato ligand coordination distorted the expected D_{4h} symmetry to approximate a D_{2h} symmetry, splitting of the Q band into Q_x and Q_y components is perfectly feasible. We conclude that D_{4h} symmetry distortion does not have to be pronounced to generate measurable Q-band splittings into a Q_x and Q_y component as observed in **1**−**8**, **15**, and **16**. Related to their general high solubility in organic solvents, phthalocyanine complexes **1**−**8** showed no aggregation in THF up to 5 μM concentrations. Rather, it followed the Beer−Lambert law ($A = \varepsilon Cl$ with A = absorbance, ε = extinction coefficient, C = concentration, and l = path length = 1 cm) as absorbance correlated linearly with concentration (Figure 3) up to 5 μM.

Electrochemistry. Cyclic voltammetry (CV), linear sweep voltammetry (LSV), and Osteryoung square-wave voltammetry (OSW) were conducted on **1**−**8** as well as **15** and **16** in dry CH_2Cl_2 utilizing 0.2 mol dm^{-3} $[N(^nBu)_4][B(C_6F_5)_4]$ as supporting electrolyte. This solvent is known to minimize solvent−compound interactions, while the electrolyte mimimises ionic interactions of the type $(\text{cations})^{n+}\cdots^{-}[B(C_6F_5)_4]$.[32] Data for cyclic voltammetry experiments are summarized in Table 3; CVs are shown in Figures 4 and 5.

Except for the diferrocenyl complexes **4** and **8**, four of the possible six phthalocyanine ring-based redox processes labeled in Roman numerals I−V could be observed; **4** and **8** showed only three. All ferrocene-based redox processes F1−F4 could also be observed, and strikingly, they were well resolved. That these ferrocenyl peaks were well resolved stems from the use of the $CH_2Cl_2/[N(^nBu)_4][B(C_6F_5)_4]$ solvent/supporting electrolyte system. Peak potentials of the corresponding Hf and Zr complexes were almost the same. Potentials of corresponding

dx.doi.org/10.1021/ic302730v | Inorg. Chem. 2013, 52, 10245−10257

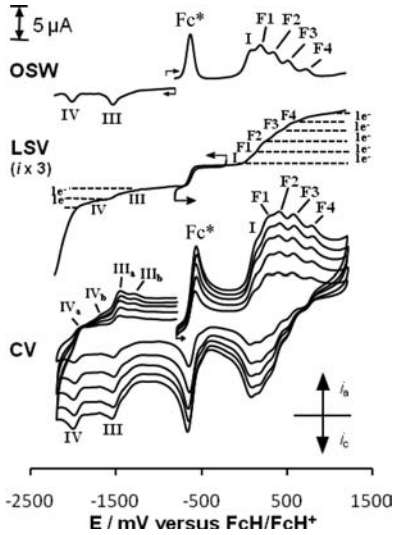

Figure 4. Osteryoung square wave voltammograms at 10 Hz (top), linear sweep at 2 mV/s (middle), and cyclic voltammograms (bottom) of **8** in CH_2Cl_2/0.2 mol dm^{-3} $[N(^nBu)_4][B(C_6F_5)_4]$ on a glassy carbon-working electrode at scan rates of 100, 200, 300, 400, and 500 mV/s. Decamethylferrocene, Fc*, was used as internal standard, but potentials are referenced FcH/FcH^+. Arrows show the onset potential and scan direction. Current of the LSV experiment was scaled by a factor of 3 to afford better interpretation.

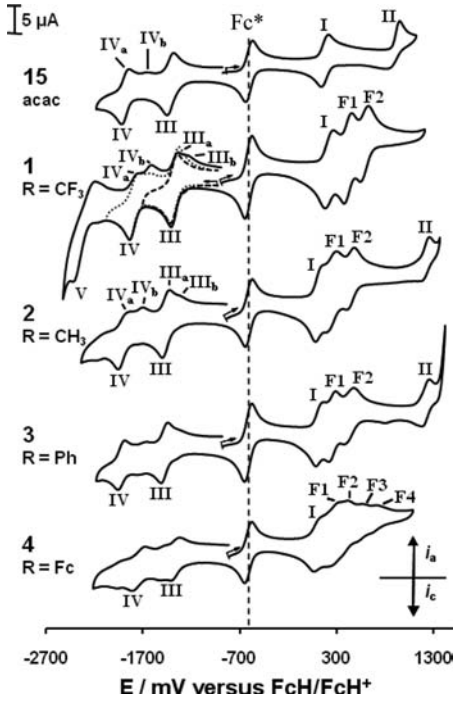

Figure 5. Cyclic voltammograms of ca. 0.5 mmol dm^{-3} solutions of $PcZr(FcCOCHCOR)_2$ **1**–**4** at 100 mVs^{-1} in CH_2Cl_2/0.2 mol dm^{-3} $[N(^nBu)_4][B(C_6F_5)_4]$ at 20 °C. $PcZr(CH_3COCHCOCH_3)_2$, **15**, is included for comparison. Dotted and dashed graphs in **1** represent CVs in which the switching potential was set to exclude either wave V or wave IV. This resulted in a substantial decrease in peak currents of wave IV_b, while wave III_b was totally eliminated.

redox processes for the Zr complexes with only a few exceptions were within 15 mV of that of the Hf complexes, Table 3. The second ring-based reduction, wave IV, or in the case of **1** vs **5**, the third ring-based reduction, wave V, showed the biggest difference in $E^{\circ\prime}$ values (30–62 mV). In oxidative processes (waves I, II, and the ferrocenyl waves), the difference between $E^{\circ\prime}$ values for Hf and Zr complexes were, with one exception, even less. The exception, complex **8**, exhibited a 57 mV larger $E^{\circ\prime}$ value for wave F4 than complex **4**.

As with the ferrocene-free compounds described in the Tomachynski–Kadish collaboration,[16c] at least two ring-based reduction waves labeled IV and III could be observed for all complexes within the negative potential limit CH_2Cl_2 allows, while the CF_3 complexes **1** and **5** showed a third redox couple, wave V, Figure 5. From the literature,[16c] when the electron-donating ferrocenyl group is replaced with a phenyl group, the CF_3 complexes exhibit four reduction processes. Except for **15** and **16**, all other Tomachynski compounds showed three reduction processes.[16c] Our results, like the crystal structure of **7** suggested, indicate that the electron-withdrawing CF_3 group of the axial β-diketonato ligands communicate through the Hf and Zr center with the macrocycles. The electron-withdrawing capability of the CF_3 group is the largest (χ_{CF3} = 3.01) of all β-diketonato R groups[25] and therefore will withdraw the most electron density from the macrocycle through the Zr/Hf metal center. For the CF_3 complexes **1** and **5**, so much electron density was removed from the macrocyclic rings that the third ring-based reduction couple moved into the potential window in which CH_2Cl_2 allows electrochemical measurements. Wave V represented an electrochemical irreversible process in both **1** and **5** as ΔE_p > 220 mV even at slow (100 mV s^{-1}) scan rates. Theoretically, electrochemical reversibility is characterized by ΔE_p values of 59 mV.[33,34] In general, peak positions III–V of **1**–**8**, **15**, and **16** moved to higher or lower potential values in a manner that is dependent on the combined electron-withdrawing or electron-donating effect of the pendent side groups R, Fc, or CH_3 on the macrocycle. These potential shifts in $E^{\circ\prime}$ values could be mathematically quantified (Figure 7) and are discussed below.

The third reduction wave of **1**, wave V, showed the typical features of analyte electrode deposition because, upon reduction, i_{pc} for this wave was much larger compared to either i_{pa} or i_{pc} of the other waves (wave V i_{pa}/i_{pc} = 0.65). This led to the distorted shape of wave V in Figure 5 compared to the ideal CV shape as exhibited by the Fc* wave.

Waves IV and III showed signs of E_{pa} peak splitting into IV_a and IV_b as well as III_a and III_b components, Figures 4 and 5, during the anodic half cycle. This feature was most prominent in **1**, **2**, **5**, **6**, and **16**, although the other complexes also showed this effect to a limited extent. In contrast, upon changing the switching potential to values that excluded wave IV, wave III had the normal CV shape with no peak splitting in the anodic half cycle. This is demonstrated in Figure 5 for complex **1**. It follows that the electrochemistry associated with wave IV is the source of this split in anodic wave III. However, when the switching potential was adjusted to exclude wave V, wave IV_b was not eliminated but only became smaller.

There are three possible explanations for the observed anodic peak split at waves III and IV. The first may be linked to the complexes themselves in that the axial β-diketonato ligands may isomerize during the second reduction (i.e., at wave IV) into different geometries. Although it is quite clear that different isomers may exist in solution (see ^1H NMR discussion above), we do not consider this as a major contributing reason for the observed anodic peak splits at waves III and IV because complexes **15** and **16** bearing the symmetric acac axial ligands also very clearly show this peak splitting. Apparently the

dx.doi.org/10.1021/ic302730v | Inorg. Chem. 2013, 52, 10245–10257

possible different isomers have a large effect on ^{1}H NMR spectra, but in view of the good ΔE values observed (Table 3), they have little or no effect on the redox potentials of **1**−**8**, **15**, and **16**. Second, compound deposition on the electrode during reduction at wave IV potentials may give rise to the observed peak splitting. However, unlike wave V for **1**, wave IV i_{pc} values for all complexes were very close to the i_{pc} values of all other peaks, which are consistent with no significant electrode fouling due to electrode deposition at wave IV reduction. The third and more likely explanation for anode peak splitting of waves IV and V is product dimerization after the second reduction at wave IV occurred. Self-association of oxidized or reduced metal-containing phthalocyaninato macrocycles is not unknown, and we reported extensively on this phenomena utilizing cadmium phthalocyanines.[35] A crystal structure of a trimeric associated cadmium species was also described.[36] The reduction behavior of **1**−**8**, **15**, and **16** is consistent with dimerization as shown in Scheme 2.

Scheme 2. Mechanism Explaining the Reducing Electrochemistry of 1−8, 15, and 16[a]

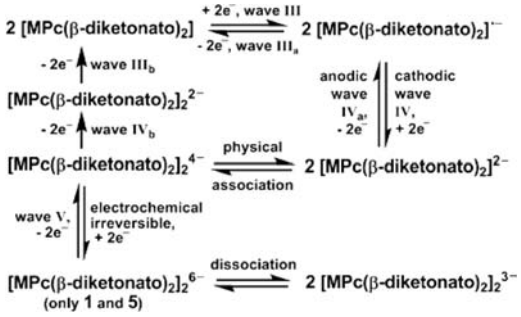

[a]Each step represents a one-electron transfer per molecular fragment. Only complexes **1** and **5** also show wave V. M = Zr or Hf.

The relative intensity of waves IV_a and IV_b as well as waves III_a and III_b will depend on (a) how slow the equilibrium involving self-association is and (b) what the equilibrium constant of this equilibrium is. Peaks IV_a and IV_b as well as III_a and III_b were in general approximately 200−250 mV apart.

It is not clear whether **1** and **5** after wave V reduction still exists as a dimer, as no clear anodic peak splitting for wave V was observed. The large negative charge (6−) does argue in favor of dimer break up due to repulsive forces, although in our cadmium studies a trimer having charge −11 was found to be feasible on CV time scale.[35,36]

The peak current ratios of waves IV deviated from unity depending on how intense peak IV_b was (Table 2), while that of wave III approached unity if the switching potential was chosen such that wave IV was not observed.

The oxidation behavior of **1**−**8**, **15**, and **16** manifested in one or two ring-based oxidations I and II and successive ferrocenyl oxidations labeled F1−F4 (Figures 4 and 5). This contrasts the two or three oxidations observed by Tomachynski and Kadish[16c] and is a direct consequence of the influence of the electron-withdrawing Fc^+ group on the ring-based oxidation redox processes of our compounds. All oxidations were electrochemically reversible at slow (100 mV s^{-1}) scan rates with ΔE < 90 mV and, excluding the redox process associated with wave II, chemically reversible with peak current ratios approaching unity, Table 3. That the first ring-based oxidation observed at wave I occurs before the ferrocenyl-based oxidations was confirmed by spectroelectrochemistry and is discussed below. The HOMO−LUMO gap expressed by $\Delta E^{\circ\prime}_{\text{I–III}} = \Delta E^{\circ\prime}_{\text{wave I}} - \Delta E^{\circ\prime}_{\text{wave III}}$ (Table 1) averaged 1.600 V, which is within the $\Delta E^{\circ\prime}_{\text{I–III}}$ = 1.56−1.67 V range observed for other Zr and Hf phthalocyanines.[16c] This shows that the presence of the ferrocenyl groups on axial β-diketonato ligands does not excessively influence the HOMO−LUMO gap for the first reduction and first oxidation ring-based redox processes.

The second ring-based oxidation associated with wave II was only observed for **2**, **3**, **6**, **7**, **15**, and **16** because for these complexes the electron density of the phthalocyaninato macrocycle was large enough that this redox process occurred in the potential window that the solvent CH_2Cl_2 allows. However, for **1**, **4**, **5**, and **8**, the two CF_3 substituents (χ_{CF3} = 3.01) or the four (oxidized) ferrocenium groups (Fc^+ = $(C_5H_5)Fe^{III}(C_5H_4)$ with χ_{Fc+} = 2.82) withdrew so much electron density from the phthalocyaninato macrocycle that the second ring-based oxidation fell outside the usable potential window of CH_2Cl_2. This results also confirms good through-bond electronic communication between β-diketonato pendent side groups (Fc or R) and the phthalocyaninato macrocycle. Because of this good communication, the observed redox potentials associated with all oxidative peaks were also dependent on the sum of the β-diketonato pendent side group electronegativities, $\Sigma\chi_R$. This is discussed and mathematically quantified, see Figure 7.

The extraordinary resolution of the ferrocenyl-based waves is the result of good through-bond communication between differently charged ferrocenyl groups in partially oxidized intermediates and also use of the CH_2Cl_2/$[N(^nBu)_4][B(C_6F_5)_4]$ solvent/supporting electrolyte system which minimizes ion pair formation of the type $(cation)^{n+}\cdots^{-}[B(C_6F_5)_4]$. The pioneering research of especially Geiger[32,37] highlights the beneficial effects that can be obtained using this solvent/electrolyte system. During the oxidation of each ferrocenyl group, mixed-valent species are formed, Scheme 3. The groups electronegativity of the neutral ferrocenyl group is χ_{Fc} = 1.87, and that of the positively charged ferrocenium group is χ_{Fc+} = 2.82.[25] As **1**−**8** becomes progressively more oxidized, the electron-withdrawing effect of each positively charged ferrocenium group is transmitted via through-space electrostatic field effects[38] and also via through-bond field effects via the

Scheme 3. Oxidation Processes for 3 Highlighting the Active Redox Site for Each Process[a]

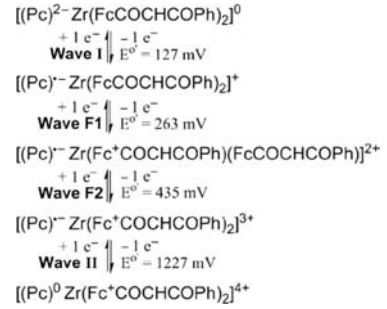

[a]Zr is charged 4+. Each β-diketonato ligand has in itself a single negative charge prior to Fc oxidation, and the phthalocyaninato ring has in the resting state a charge of 2−. Charges shown adjacent to the Pc ring round brackets represent the overall charge on the Pc ring, and the charge outside the square brackets represents the overall molecular charge.

delocalized β-diketonato bonds described in the crystallographic section above to the remaining yet-to-be oxidized ferrocenyl groups. The result of this good electronic communication causes the remaining ferrocenyls to become progressively more difficult to oxidize. In the case of **4** and **8**, this resulted in the observed 392 or 511 mV span of ferrocenyl formal oxidation potentials for peaks F1−F4 (Table 3). Different formal reduction potentials for symmetrical complexes in which mixed-valent redox-active intermediates are generated (here, for example $\mathbf{4}^{+}$, $\mathbf{4}^{2+}$, $\mathbf{4}^{3+}$, $\mathbf{4}^{4+}$, and $\mathbf{4}^{5+}$, respectively) are well known in systems that allow through-bond electronic communication between these molecular fragments.[39]

The Osteryoung square wave voltammetry (OSV) showed enhanced resolution of waves I and F1−F4 and II, Figure 4, and linear sweep voltammetry (LSV) showed that each redox wave in **1**−**8**, **15**, and **16** represents the same number of electron flow, namely, a one-electron transfer process.

Spectroelectrochemistry of [PcZr(FcCOCHCOCF$_3$)$_2$], 1. To decide whether the first observed oxidation wave was that of the first ring-based Pc/Pc$^+$ oxidative couple (i.e., wave I) or whether it was the first Fc/Fc$^+$ couple of one of the β-diketonato ligands (i.e., wave F1), three approaches are relevant. The first relates to Figure 7 (next section) that demonstrates the good relationship between $\Sigma\chi_R$ and $E^{\circ\prime}$ for waves series I and F. If the assignment of waves I and F1 were the wrong way around, then the points of wave I ferrocene-free derivatives **15** and **16** is completely off the wave I line. The good fit for all other points on lines associated with waves F and I (Figure 7) argues completely against this.

Second, consideration of the HOMO−LUMO gap of phthalocyanines having redox-silent metals coordinated in its central cavity, here Zr^{4+} and Hf^{4+}, is also relevant. The difference between $E^{\circ\prime}$ of the first oxidation process (wave I) and $E^{\circ\prime}$ for the first reduction process (wave III) is directly related to the HOMO−LUMO energy gap for metallophthalocyanines having redox-silent metal centers (zirconium and hafnium in this case).[40] The energy of the Q-band absorption is also related to the Q-band λ_{max} value[40] via the equation $E = hc/\lambda$. Since the Q-band absorption wavelength for the ferrocene-free acac-containing complexes **15** and **16** are for all practical purposes observed at the same wavelength as those of the ferrocene-containing complexes **1**−**8**, it can be concluded that the energies of the HOMO−LUMO gaps are almost the same for all these complexes. Therefore, the $\Delta E^{\circ\prime}_{\text{I–III}} = E^{\circ\prime}_{\text{wave I}} - E^{\circ\prime}_{\text{wave III}}$ potential differences should be closely the same for **1**−**8**, **15**, and **16**. By comparing the UV−vis Q-band absorption wavelength of PcZr(CH$_3$COCHCOCH$_3$)$_2$ (**15**, $\lambda_{max,Qx}$ = 677 nm and $\lambda_{max,Qy}$ = 687 nm, Table 1) with that of ferrocenyl-containing PcZr(FcCOCHCOCH$_3$)$_2$ (**2**, $\lambda_{max,Qx}$ = 681 nm and $\lambda_{max,Qy}$ = 687 nm) it is clear that they have similar HOMO−LUMO gap energies (because λ_{max} values are almost the same). Since the central zirconium metal is redox silent in the studied potential range, it translates that the $\Delta E^{\circ\prime}_{\text{I–III}}$ potential difference for these complexes should be closely the same. Macrocycle- (waves I−V) and ferrocenyl-based (waves F1−F4) formal reduction potentials, $E^{\circ\prime}$, are summarized in Table 1. The $\Delta E^{\circ\prime}_{\text{I–III}}$ potential difference of **15** was found to be 1.598 V (Table 1). For **2** there are 3 possibilities to calculate $\Delta E^{\circ\prime}_{\text{I–III}}$. One has to use either the first oxidation wave, labeled I giving $\Delta E^{\circ\prime}_{\text{I–III}}$ = 1.593 V, or the second, which is wave F1; then $\Delta E^{\circ\prime}_{\text{Fc1–III}}$ = 1.714 V, or the third oxidation redox process observed, which is wave F2 giving $\Delta E^{\circ\prime}_{\text{Fc2–III}}$ = 1.908 V. From these three possible $\Delta E^{\circ\prime}$ potentials it can be concluded that the only viable option is when the first oxidation process is macrocycle based, as assigned in the electrochemical discussion above. This then is followed by the two ferrocenyl-based processes F1 and F2. A similar treatment of data has also been applied to all other complexes, $\Delta E^{\circ\prime}$ values are summarized in Table 1. The close agreement of $\Delta E^{\circ\prime}_{\text{I–III}}$ values for all complexes inclusive of **15** and **16** is apparent ($1.589 \le \Delta E^{\circ\prime}_{\text{I–III}} \le 1.611$ V) and consistent with the assignment of wave I to the first ring-based oxidation of each macrocycle and NOT to the first ferrocene-based oxidation of complexes **1**−**8**.

To experimentally confirm the redox process assignment of wave I as belonging to the first ring-based oxidation of each macrocycle as described above, complex PcZr(FcCOCHCOCF$_3$)$_2$, **1**, was analyzed by means of spectroelectrochemistry using a optically transparent thin-layer electrochemical (OTTLE) cell with CaF_2 windows 2 mm apart, a platinum minigrid working electrode, a platinum wire auxiliary electrode, and a silver wire reference electrode. Complex **1** was chosen for this experiment as it has the best resolution between the three redox waves I, F1, and F2 in the 0−700 mV range (versus FcH/FcH$^+$, values as per Table 3).

The cyclic voltammogram obtained by employing the OTTLE cell for 0.125 mM solutions of **1** in CH_2Cl_2 (Supporting Information) showed three anodic peak potentials vs Ag wire (not FcH/FcH$^+$) at 640, 875, and 1050 mV.

When a potential of 0.4 V vs Ag wire was applied to the OTTLE cell (i.e., a potential substantially smaller than the $E^{\circ\prime}$ of wave I) almost no spectral changes were observed in the UV−vis spectrum of **1**, Figure 6. This was consistent with a potential that is too small to induce any oxidation. Upon applying a potential larger than $E^{\circ\prime}$ of wave I but smaller than E_{pa} of wave F1, $E_{applied}$ = 700 mV vs Ag wire, the Q band was almost destroyed completely (Figure 6). The spectral changes observed reproduce the spectral changes of nonferrocene-containing β-diketonato Zr and Hf phthalocyaninato complexes very well.[16c] Tomachynski and Kadish identified in their spectroelectrochemical study on a thio-substituted acac derivative coordinated to Hf that a band at 851 nm forms,

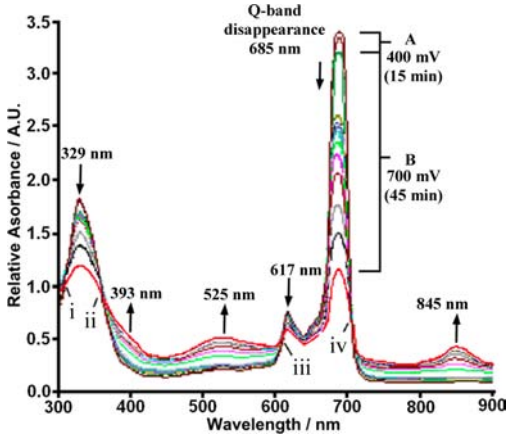

Figure 6. UV−vis spectral changes for a 0.125 mmol dm^{-3} solution of **1** in CH_2Cl_2 upon applying 400 and 700 mV vs Ag wire to an OTTLE cell in the presence of 0.025 mol dm^{-3} [N(^{n}Bu)$_4$][B(C$_6$F$_5$)$_4$] as supporting electrolyte. Points labeled i (at 313 nm), ii (383 nm), iii (614 nm), and iv (713 nm) are isosbestic points that were observed during electrochemical oxidation of **1** that resulted in diminishing of the Q band.

dx.doi.org/10.1021/ic302730v | Inorg. Chem. 2013, 52, 10245−10257

the Q band at 692 and 680 nm disappears, a band at 617 nm disappears, a band at 520 nm forms, a band at 383 nm forms, and a B (Sorret) band at 341 nm disappears or changes intensity upon oxidation. In our case, oxidation of the trifluoro ferrocenyl β-diketonato complex of Zr, complex **1**, followed exactly the same trend at peaks with maximum wavelengths 845, 689, 681, 617, 525, 393, and 329 nm. We conclude that our spectroelectrochemical result is consistent with a ring-based oxidation assignment for wave I and not with a ferrocenyl assignment. If wave I oxidation was associated with the ferrocenyl groups rather than the macrocyclic ring, the Q band would shift to another λ_{max} value.[41]

Allthough this study has not focused on reductive spectroelectrochemical studies, reductive spectroelectrochemical studies on structually related complexes may be found in the Tomachynski–Kadish work.[16c]

Quantification of the Relationship between $\Sigma\chi_R$ and $E^{\circ\prime}$. It was previously shown that $E^{\circ\prime}$ can be expressed linearly as a function of the sum of group electronegativities in complexes of the type $[Rh(FcCOCHCOR)(CO)_2]$,[42] $[Rh(FcCOCHCOR)CO(PPh_3)]$,[43] and $[Rh(FcCOCHCOR)(cod)]$[19b] and also as the sum of the group electronegativities of four meso substituents, $\Sigma\chi_R = \chi_{R1} + \chi_{R2} + \chi_{R3} + \chi_{R4}$, for porphyrins.[44] In all these complexes, good communication exists between molecular fragments. We show here for the first time that the sum of group electronegativities of β-diketonato pendant side groups when axially coordinated to metal phthalocyanines may also be used to predict phthalocyaninato redox potentials. To explain the approach that was used, consider peak F2 of $PcZr(FcCOCHCOCF_3)_2$, **1**. Peak F2 represents the couple

$$[(Pc)^{\bullet-}Zr(Fc^{+}COCHCOCF_3)(FcCOCHCOCF_3)]^{2+}$$

Wave F2, $E^{\circ\prime} = 590$ mV, $+1\,e^{-}$ / $-1\,e^{-}$

$$\mathbf{1}^{2+}$$

$$[(Pc)^{\bullet-}Zr(Fc^{+}COCHCOCF_3)_2]^{3+}$$

$$\mathbf{1}^{3+}$$

Then for $\mathbf{1}^{2+}$

$$\begin{aligned}\Sigma\chi_R &= (\chi_{Fc} + \chi_{CF3}) + (\chi_{Fc+} + \chi_{CF3})\\ &= (1.87 + 3.01) + (2.82 + 3.01)\\ &= 10.71\end{aligned}$$

Similarly, a measure of the electron density on $\mathbf{1}^{3+}$ that is to be oxidized at wave II is $\sum\chi_R = 11.66$. The quantity $\Sigma\chi_R$ was calculated for all electrochemically observed intermediates for all complexes.

Figure 7 shows the relationship between $\sum\chi_R$ and $E^{\circ\prime}$ for each macrocycle-based redox process as well as the ferrocenyl processes for compounds **1**–**8**, **15**, and **16**. For each redox process, a linear relationship between $E^{\circ\prime}$ and $\sum\chi_R$ was observed. The equations predicting $E^{\circ\prime}$ (V) from $\sum\chi_R$ for **1**–**8** for each wave I–IV and F were found to be

$$\mathbf{IV}: E^{\circ\prime} = 0.054\sum\chi_R - 2.347 \quad (R^2 = 0.7936) \tag{1}$$

$$\mathbf{III}: E^{\circ\prime} = 0.048\sum\chi_R - 1.854 \quad (R^2 = 0.9396) \tag{2}$$

$$\mathbf{I}: E^{\circ\prime} = 0.047\sum\chi_R - 0.242 \quad (R^2 = 0.8791) \tag{3}$$

$$\mathbf{II}: E^{\circ\prime} = 0.333\sum\chi_R - 2.201 \quad (R^2 = 0.9349) \tag{4}$$

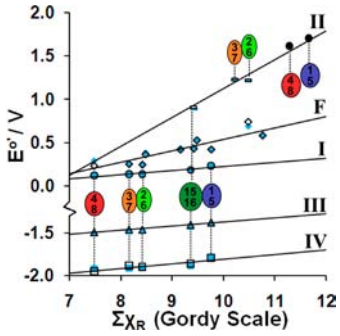

Figure 7. Linear relationship between the sum of the group electronegativities of β-diketonato pendant R groups, $\Sigma\chi_R$, and the formal redox potentials $E^{\circ\prime}$ for the ferrocenyl redox processes (wave series F) and the phthalocyaninato ring-based processes associated with waves I, II, III, and IV. Compound numbers are given in each circle. Solid blue markers indicate Zr complexes, while hollow black markers indicate Hf complexes. Points that have the appearance of a blue marker encaged in a black border are points where the Hf and Zr data overlap. Solid black markers indicate expected positions for wave II of complexes **1**, **4**, **5**, and **8**.

$$\mathbf{F}: E^{\circ\prime} = 0.1323\sum\chi_R - 0.7835 \quad (R^2 = 0.8011) \tag{5}$$

Wave II of complexes **1**, **4**, **5**, and **8** was not experimentally observed because it fell outside the potential window of the solvent. However, utilizing eq 4, the value for these complexes could now be predicted. They are estimated as approximately 1.62(5) V for **4** and **8** (R = Fc) as well as 1.71(6) V for **1** and **5** (R = CF_3).

CONCLUSIONS

$[PcM(R^1COCHCOR^2)_2]$ complexes **1**–**8**, **15**, and **16** with M = Zr, Hf and substituents R^1 = Fc or CH_3 and R = CF_3, CH_3, Ph, and Fc were synthesized. The structure of $PcHf(FcCOCHCOPh)_2$, **7**, was solved and gave clear indications by means of delocalized bond lengths that good communication between pendant β-diketonato substituents and the phthalocyaninato ring should exist. The observed distortion of the expected D_{4h} symmetry of the phthalocyaninato coordination site explains the Q-band splitting into Q_x and Q_y components with $3 \le \Delta\lambda_{max} \le 10$ nm. The observed Q-band peak splitting resembled Q-band peak patterns for metal-free phthalocyanines, although then $\Delta\lambda_{max} \approx 30$ nm, where D_{4h} symmetry is lifted to become D_{2h}. From an electrochemical study it was possible to resolve all the Fc/Fc^+ couples of **1**–**8** in the formal reduction potential range $236 < E^{\circ\prime} < 745$ mV vs FcH/FcH^+. Spectroelectrochemical evidence, UV–vis Q-band maximum wavelengths, and HOMO–LUMO energy gaps as expressed by $\Delta E^{\circ\prime}{}_{I-III} = \Delta E^{\circ\prime}{}_{wave\ I} - \Delta E^{\circ\prime}{}_{wave\ III}$ values were mutually consistent in indicating that the first ring-based oxidation occurs before ferrocenyl oxidations take place. The Zr and Hf centers are redox silent and exert comparable influences on the redox potentials in complexes **1**–**8**, **15**, and **16**. The $E^{\circ\prime}$ potentials of all ferrocenyl and ring-based redox couples were observed to increase linearly with an increase in the sum of the group electronegativity $\Sigma\chi_R$ of the pendant R groups of the axial β-diketonato ligands; the relationship between $E^{\circ\prime}$ and $\Sigma\chi_R$ could mathematically be quantified for each of the four observed ring-based redox processes as well as for the ferrocenyl-based redox processes. This allowed prediction of potentials for redox processes that fall outside the workable potential window of the solvent, here CH_2Cl_2.

dx.doi.org/10.1021/ic302730v | Inorg. Chem. 2013, 52, 10245–10257

EXPERIMENTAL SECTION

General Information. Solid reagents (ferrocene, $ZrCl_4$, and $HfCl_4$; Aldrich) were used without any further purification. Organic solvents were dried according standard methods or distilled directly prior to use where specified. Doubly distilled water was used. Column chromatography was performed on Kieselgel 60 (Merck, grain size 0.040−0.063 nm) using hexane:diethyl ether (1:1) as mobile phase unless otherwise specified. Ferrocene-containing β-diketones $FcCOCH_2COR$ with R = CH_3 (**11**), CF_3 (**12**), Ph (**13**), and Fc, **14**) were synthesized utilizing published methods with care being taken to separate it from the aldol self-condensation product of acetyl ferrocene, $FcCOCH{=}C(CH_3)Fc$.[25,45] Precursors $PcZrCl_2$ and $PcHfCl_2$ and $[PcM(acac)_2]$ complexes **15** and **16** were synthesized as described before.[16a] The electrolyte $[N(^nBu)_4][B(C_6F_5)_4]$ was synthesized according to the procedure described by Geiger.[37] ^1H NMR spectra at 20 °C were recorded on a Bruker Advance DPX 300 NMR spectrometer at 300 MHz with chemical shifts presented as δ values referenced to $SiMe_4$ at 0.00 ppm utilizing $CDCl_3$ as solvent. Elemental analyses were performed either by the University of the Free State's Analytical Chemistry division using a Leco Truspec Micro instrument for C, H and N analysis or by Canadian Microanalytical Service, Delta, British Columbia, Canada.

Synthesis of 1−8. All complexes were prepared according to the same procedure; synthesis of **1** may serve as an example.

Bis-(1-ferrocenyl-4,4,4-trifluorobutane-1,3-dionato-κ²-O,O′)-zirconium(IV) phthalocyanine, 1. $PcZrCl_2$ (356.5 mg, 0.53 mmol) was suspended in toluene (10 mL), and solid 1-ferrocenyl-4,4,4-trifluorobutane-1,3-dione (2.2 eq., 376.7 mg, 1.16 mmol) was added to the mixture. The reaction mixture was heated at reflux for 4 h. The hot reaction mixture was filtered, and the obtained solution was cooled to room temperature. *n*-Hexane (200 mL) was added to the solution, and the mixture was cooled to −25 °C for 18 h to precipitate the product. The precipitate was filtered off and washed with *n*-pentane until washings were colorless. The precipitate was first air dried and then finally dried under vacuum (<580 mmHg) at 60 °C for 8 h to give 349 mg of **1** in 52.7% yield. Mp > 350 °C. ^1H NMR δ_H (300 MHz, $CDCl_3$)/ppm: 9.75−9.25 (m, 8H, 8 × Ar−H^{α}), 8.45−8.05 (m, 8H, 8 × Ar−H^{β}), 4.76−4.68 (s, 2H, 2 × CH), 4.41−3.53 (m, 18H, 2 × C_5H_5, 2 × C_5H_4). Anal. Calcd for $C_{60}H_{36}F_6Fe_2N_8O_4Zr$: C, 57.66; H, 2.90; Fe, 8.94; N, 8.97; Zr, 7.30. Found: C, 57.16; H, 3.33; Fe, 7.96; N, 9.11; Zr, 8.35.

Characterization Data for 2−8. *Bis-(1-ferrocenylbutane-1,3-dionato-κ²-O,O′)zirconium(IV) Phthalocyanine, 2.* Complex **2** was prepared from $PcZrCl_2$ (397 mg, 0.59 mmol) and 1-ferrocenylbutane-1,3-dione (2.2 equiv, 350 mg, 1.30 mmol) in toluene (10 mL). Yield **2**: 13.6% (91.6 mg, 0.08 mmol). Mp > 350 °C. ^1H NMR δ_H (300 MHz, $CDCl_3$)/ppm: 9.75−9.30 (m, 8H, 8 × Ar−H^{α}), 8.35−8.04 (m, 8H, 8 × Ar−H^{β}),4.52−4.47 (s, 2H, 2 × CH), 4.26−3.48 (m, 18H, 2 × C_5H_5, 2 × C_5H_4), 1.32 (m, 6H, 2 × CH_3). Anal. Calcd for $C_{60}H_{42}Fe_2N_8O_4Zr$: C, 63.11; H, 3.71; Fe, 9.78; N, 9.81; Zr, 7.99. Found: C, 62.67; H, 4.12; Fe, 8.95; N, 9.44; Zr, 9.41.

Bis-(1-ferrocenyl-3-phenyl-1,3-propanedionato-κ²-O,O′)-zirconium(IV) Phthalocyanine, 3. Complex **3** was prepared from $PcZrCl_2$ (220 mg, 0.33 mmol) and 1-ferrocenyl-3-phenyl-1,3-propanedione (2.2 equiv, 238 mg, 0.72 mmol) in toluene (10 mL). Yield **3**: 41.3% (172.5 mg, 0.136 mmol). Mp > 350 °C. ^1H NMR δ_H (300 MHz, $CDCl_3$)/ppm: 9.74−9.08 (m, 8H, 8 × Ar−H^{α}), 8.45−7.98 (m, 8H, 8 × Ar−H^{β}), 7.53−6.88 (m, 10H, 2 × C_6H_5), 5.22−5.16 (s, 2H, 2 × C*H*), 4.28−3.29 (m, 18H, 2 × C_5H_5, 2 × C_5H_4). Anal. Calcd for $C_{70}H_{46}Fe_2N_8O_4Zr$: C, 66.41; H, 3.66; Fe, 8.82; N, 8.85; Zr, 7.21. Found: C, 66.16; H, 4.23; Fe, 7.66; N, 8.42; Zr, 8.37.

Bis-(1,3-diferrocenylpropane-1,3-dionato-κ²-O,O′)zirconium(IV) Phthalocyanine, 4. Complex **4** was prepared from $PcZrCl_2$ (136.6 mg, 0.20 mmol) and 1,3-diferrocenylpropane-1,3-dione (2.2 equiv, 196 mg, 0.45 mmol) in toluene (10 mL). Yield **4**: 32.9% (98.4 mg, 0.066 mmol). Mp > 350 °C. ^1H NMR δ_H (300 MHz, $CDCl_3$)/ppm: (poor solubility): 9.74−9.50 (m, 8H, 8 × Ar−H^{α}), 8.41−8.18 (m, 8H, 8 × Ar−H^{β}), 5.38 (s, 2H, 2 × CH), 4.44−3.50 (m, 36H, 4 × C_5H_5, 4 × C_5H_4). Anal. Calcd for $C_{78}H_{54}Fe_4N_8O_4Zr$: C, 63.22; H, 3.67; Fe, 15.07; N, 7.56; Zr, 6.16. Found: C, 61.53; H, 4.11; Fe, 14.04; N, 7.84; Zr, 8.71.

Bis-(1-ferrocenyl-4,4,4-trifluorobutane-1,3-dionato-κ²-O,O′)-hafnium(IV) Phthalocyanine, 5. Complex **5** was prepared from $PcHfCl_2$ (350 mg; 0.46 mmol) and 1-ferrocenyl-4,4,4-trifluorobutane-1,3-dione (2.2 equiv; 327.3 mg; 1.02 mmol) in toluene (10 mL). Yield **5**: 71.4% (439.4 mg; 0.33 mmol). Mp > 350 °C. ^1H NMR δ_H (300 MHz, $CDCl_3$)/ppm: 9.75−9.27 (m, 8H, 8 × Ar−H^{α}), 8.45−8.06 (m, 8H, 8 × Ar−H^{β}), 4.73−4.63 (s, 2H, 2 × CH), 4.41−3.50 (m, 18H, 2 × C_5H_5, 2 × C_5H_4). Anal. Calcd for $C_{60}H_{36}F_6Fe_2HfN_8O_4$: C, 53.89; H, 2.71; Fe, 8.35; Hf, 13.35; N, 8.38. Found: C, 53.05; H, 3.59; Fe, 7.64; Hf, 14.34; N, 8.41.

Bis-(1-ferrocenylbutane-1,3-dione-κ²-O,O′)hafnium(IV) Phthalocyanine, 6. Complex **6** was prepared from $PcHfCl_2$ (324.6 mg; 0.426 mmol) and 1-ferrocenylbutane-1,3-dione (2.2 equiv, 253.1 mg, 0.937 mmol) in toluene (10 mL). Yield **6**: 55.8% (292.1 mg, 0.238 mmol). Mp > 350 °C. ^1H NMR δ_H (300 MHz, $CDCl_3$)/ppm: 9.76−9.28 (m, 8H, 8 × Ar−H^{α}), 8.41−8.02 (m, 8H, 8 × Ar−H^{β}), 4.48−4.41 (s, 2H, 2 × CH), 4.29−3.42 (m, 18H, 2 × C_5H_5, 2 × C_5H_4), 1.34−1.24 (s, 6H, 2 × CH_3). Anal. Calcd for $C_{60}H_{42}Fe_2HfN_8O_4$: C, 58.63; H, 3.44; Fe, 9.09; Hf, 14.52; N, 9.12. Found: C, 59.74; H, 3.23; Fe, 8.29; Hf, 14.80; N, 7.43.

Bis-(1-ferrocenyl-3-phenyl-1,3-propanedionato-κ²-O,O′)hafnium-(IV) Phthalocyanine, 7. Complex **7** was prepared from $PcHfCl_2$ (308.3 mg, 0.405 mmol) and 1-ferrocenyl-3-phenyl-1,3-propanedione (2.2 equiv, 295.7 mg, 0.89 mmol) in toluene (10 mL). Yield **7**: 53.3% (291.9 mg, 0.216 mmol). Mp > 350 °C. ^1H NMR δ_H (300 MHz, $CDCl_3$)/ppm: 9.78−9.03 (m, 8H, 8 × Ar−H^{α}), 8.48−7.92 (m, 8H, 8 × Ar−H^{β}), 7.59−6.87 (m, 10H, 2 × C_6H_5), 5.20−5.01 (s, 2H, 2 × CH), 4.31−3.22 (m, 18H, 2 × C_5H_5, 2 × C_5H_4). Anal. Calcd for $C_{70}H_{46}Fe_2HfN_8O_4$: C, 62.12; H, 3.43; Fe, 8.25; Hf, 13.19; N, 8.28. Found: C, 61.89; H, 4.00; Fe, 7.86; Hf, 14.95; N, 8.18. Complex **7** was recrystallized by slow evaporation−diffusion using THF as primary solvent and *n*-hexane as secondary solvent, giving deep purple crystallographic quality crystals.

Bis-(1,3-diferrocenylpropane-1,3-dionato-κ²-O,O′)hafnium(IV) Phthalocyanine, 8. Complex **8** was prepared from $PcHfCl_2$ (303.5 mg, 0.398 mmol) and 1,3-diferrocenylpropane-1,3-dione (2.2 equiv, 385.4 mg, 0.876 mmol) in toluene (10 mL). Yield **8**: 61.4% (383.2 mg, 0.244 mmol). Mp > 350 °C. ^1H NMR δ_H (300 MHz, $CDCl_3$)/ppm: (poor solubility): 9.73−9.40 (m, 8H, 8 × Ar−H^{α}), 8.39−8.16 (m, 8H, 8 × Ar−H^{β}), 5.36 (s, 2H, 2 × CH), 5.10−4.05 (m, 36H, 4 × C_5H_5, 4 × C_5H_4). Anal. Calcd for $C_{78}H_{54}Fe_4HfN_8O_4$: C, 59.70; H, 3.47; Fe, 14.24; Hf, 11.37; N, 7.14. Found: C, 59.13; H, 3.91; Fe, 15.71; Hf, 13.05; N, 6.51.

Crystal Structure Determination of 7. A deep purple crystal of **7** with approximate dimensions 0.22 × 0.13 × 0.07 mm^3 was mounted on a glass fiber and used for single-crystal X-ray diffraction analysis. Diffraction intensity data were collected on a KUMA KM4-CCD diffractometer operating in κ geometry and equipped with a two-dimensional CCD detector. Mo Kα radiation (0.71073 Å) was used. Data were collected in ω-scan mode with $\Delta\omega$ = 1.0° using the CrysAlis CCD program.[46] The CrysAlis RED software version 1.170.32 was used for data processing.[47] Empirical absorption correction was applied using spherical harmonics, implemented in the SCALE3 ABSPACK scaling algorithm. The structure was solved by direct methods and refined by the full-matrix least−squares method against F^2 by means of the SHELX-97 program package.[48] Anisotropic displacement parameters were applied for all non-hydrogen atoms. Hydrogen atoms were introduced at geometrically calculated positions and refined as riding atoms with $U_{iso}(H)$ = 1.2U_{eq} of the corresponding parent atom. Any restraints and constrains on interatomic distances and displacement parameters were introduced during refinement.

The molecular plot was drawn using the DIAMOND[49] program with a 15% thermal envelope probability for non-hydrogen atoms. Hydrogen atoms were drawn as arbitrary sized spheres with a radius of 0.15 Å.

Electrochemical Study. Cyclic voltammetry, square wave voltammetry, and linear sweep voltammetry were conducted on a

BAS 100 B/W voltammograph at 20 °C under argon utilizing a three-electrode configuration. Potentials were referenced experimentally to an Ag-wire reference electrode. Due to potential drifts during successive voltammetric measurements, each experiment had to be conducted in the presence of an internal standard, here decamethyl ferrocene, to allow manual correction of data on a spread sheet program. A glassy carbon working electrode and Pt auxiliary electrode were used.

Analyte concentrations were ca. 0.5 mM in spectrochemical grade CH_2Cl_2 (Aldrich), and 0.2 M tetrabutylammonium tetrakispentafluorophenylborate, $[N(^nBu)_4][B(C_6F_5)_4]$, was used as solvent/supporting electrolyte. Decamethylferrocene (Fc*) was used as an internal standard, but all potential values are reported against ferrocene (FcH) at 0 mV. Decamethylferrocene has $E^{\circ\prime} = -604$ mV versus free ferrocene, $i_{pc}/i_{pa} = 0.99$, and $\Delta E = 67$ mV under our conditions. Data were exported to a spread sheet program for manipulation and diagram preparation.

■ ASSOCIATED CONTENT

Supporting Information

UV−vis spectra of **5**−**10** and **16**, cif file of **7**, table with bond lengths and angles, as well as table giving additional electrochemical data at different scan rates. This material is available free of charge via the Internet at http://pubs.acs.org.

■ AUTHOR INFORMATION

Corresponding Author

*E-mail: swartsjc@ufs.ac.za.

Notes

The authors declare no competing financial interest.

■ ACKNOWLEDGMENTS

The National Research Foundation of South Africa under grant no. 81829 and the Central Research Fund of the University of the Free State are acknowledged for their financial support.

■ REFERENCES

(1) In *The Porphyrin Handbook*; Kadish, K. M.,Guilard, R., Smith, K. M., Eds.; Academic Press, Elsevier Science: New York, 2003; Vols. *15*−*20*.

(2) Leznoff, C. C.; Lever, A. B. P. In *Phthalocyanines: Properties and Applications*; VCH Publishers: New York, 1996; Vols. *1*−*4*.

(3) L' Her, M.; Pondaven, A. In *The Porphyrin Handbook*; Kadish, K. M., Guilard, R., Smith, K. M., Eds.; Academic Press, Elsevier Science: New York, 2003; Vol. *16*, pp 117−169.

(4) McKeown, N. B. In *Phthalocyanine Materials: Synthesis, Structure and Function*; Dunn, B., Goodby, J. W., West, A. R., Eds.; University Press: Cambridge, U.K., 1988.

(5) Yakuphanoglu, F.; Kandaz, M.; Yaraşir, M. N.; Şenkal, F. B. *Physica B* **2007**, *393*, 235.

(6) (a) Yilmaz, F.; Atilla, D.; Ahsen, V. *Polyhedron* **2004**, *23*, 1931. (b) Cook, M. J.; Cracknell, S. J.; Harrison, K. J. *J. Mater. Chem.* **1991**, *1*, 704.

(7) Padma, N.; Joshi, A.; Singh, A.; Deshpande, S. K.; Aswal, D. K.; Gupta, S. K.; Yakhmia, J. V. *Sensors Actuators B* **2009**, *143*, 246.

(8) (a) Haber, J.; Iwanejko, R.; Połtowicz, J.; Battioni, P.; Mansuy, D. *J. Mol. Catal. A: Chem.* **2000**, *152*, 111. (b) Yamazaki, S.; Fujiwara, N.; Yasuda, K. *Electrochim. Acta* **2010**, *55*, 753.

(9) Abdeldayem, H. A.; Frazier, D. O.; Penn, B. G.; Smith, D. D.; Banks, C. E. *Thin Solid Films* **1999**, *350*, 245.

(10) Yoshida, Y.; Nakamura, M.; Tanaka, S.; Hiromitsu, I.; Fujita, Y.; Yoshino, K. *Synth. Met.* **2006**, *156*, 1213.

(11) Vzorov, A. N.; Marzilli, L. G.; Compans, R. W.; Dixon, D. W. *Antiviral Res.* **2003**, *59*, 99.

(12) (a) Giuntini, F.; Raoul, Y.; Dei, D.; Municchi, M.; Chiti, G.; Fabris, C.; Colautti, P.; Jori, G.; Roncucci, G. *Tetrahedron Lett.* **2005**, *46*, 2979. (b) Zorlu, Y.; Dumoulin, F.; Bouchu, D.; Ahsen, V.; Lafont, D. *Tetrahedron Lett.* **2010**, *51*, 6615.

(13) (a) Conradie, J.; Swarts J. C. Ghosh, A. *J. Phys Chem. B.* **2004**, *108*, 452. (b) Conradie, J.; Wondimagegn, T.; Ghosh, A. *J. Am. Chem. Soc.* **2003**, *125*, 4968.

(14) McKeown, N. B. *J. Mater. Chem.* **2000**, *10*, 1975.

(15) Tretyakova, I. N.; Chernii, V. Ya.; Tomachynski, L. A.; Volkov, S. V. *Dyes Pigm.* **2007**, *75*, 67.

(16) (a) Tomachynski, L. A.; Tretyakova, I. N.; Chernii, V. Ya.; Volkov, S. V.; Kowalska, M.; Legendziewicz, J.; Gerasymchuk, Y. S.; Radzki, St. *Inorg. Chim. Acta* **2008**, *361*, 2569. (b) Tomachynski, L. A.; Chernii, V. Ya.; Kolotilova, Y. Yu.; Chernega, A. N.; Howard, J. A. K.; Volkov, S. V. *Inorg. Chim. Acta* **2007**, *360*, 1493. (c) Ou, Z.; Zhan, R.; Tomachynski, L. A.; Chernii, V. Ya.; Kadish, K. M. *Macroheterocycles* **2011**, *4*, 164.

(17) (a) Sarhan, A. A. O.; Izumi, T. *J. Organomet. Chem.* **2003**, *675*, 1. (b) Yang, H.; Chen, X.; Jiang, W.; Lu, Y. *Inorg. Chem. Commun.* **2005**, *8*, 853. (c) Štěpnička, P.; Solařová, H.; Císařová, I. *J. Organomet. Chem.* **2011**, *696*, 3727.

(18) (a) Ogawa, S.; Muroaka, H.; Kikuta, K.; Saito, F.; Sato, R. *J. Organomet. Chem.* **2007**, *692*, 60. (b) Hildebrandt, A.; Rüffer, T.; Erasmus, E.; Swarts, J. C.; Lang, H. *Organometallics* **2010**, *29*, 4900. (c) Chandrasekhar, V., V.; Thirumoorthi, R. *Organometallics* **2007**, *26*, 5415.

(19) (a) Conradie, J.; Swarts, J. C. *Organometallics* **2009**, *28*, 1018. (b) Conradie, J.; Swarts, J. C. *Dalton Trans.* **2011**, *40*, 5844. (c) Otto, S.; Roodt, A.; Erasmus, J. J. C.; Swarts, J. C. *Polyhedron* **1998**, *17*, 2447.

(20) Hu, X.; Bai, C.; Dai, H.; Chen, H.; Zheng, Z. *J. Mol. Catal. A: Chem.* **2004**, *218*, 107.

(21) Swarts, P. J.; Immelman, M.; Lamprecht, G. J.; Greyling, S. E.; Swarts, J. C. *S. Afr. J. Chem.* **1997**, *50*, 208.

(22) Herrmann, R.; Pedersen, B.; Wagner, G.; Youn, J.-H. *J. Organomet. Chem.* **1998**, *571*, 261.

(23) Spanig, F.; Kolvacs, C.; Hauke, F.; Ohlubo, K.; Fukuzumi, F.; Guldi, D. M.; Hirsch, A. *J. Am. Chem. Soc.* **2009**, *131*, 8180.

(24) (a) Shago, R. F.; Swarts, J. C.; Kreft, E.; Van Rensburg, C. E. J. *Anticancer Res.* **2007**, *27*, 3431. (b) Swarts, J. C.; Vosloo, T. G.; Cronje, S. J.; Du Plessis, W. C.; Van Rensburg, C. E. J.; Kreft, E.; Van Lier, J. E. *Anticancer Res.* **2008**, *28*, 2781. (c) Weber, B.; Serafin, A.; Michie, J.; Van Rensburg, C. E. J.; Swarts, J. C.; Bohm, L. *Anticancer Res.* **2004**, *24*, 763.

(25) Du Plessis, W. C.; Erasmus, J. J. C.; Lamprecht, G. J.; Conradie, J.; Cameron, T. S.; Aquino, M. A. S.; Swarts, J. C. *Can. J. Chem.* **1999**, *77*, 378.

(26) Gordy scale group electronegativities, χ_R, are empirical numbers that express the combined tendency of not only one atom but a group of atoms, like R = CF_3 or ferrocenyl (Fc), to attract electrons (including those in a covalent bond) as a function of the number of valence electrons, *n*, and the covalent radius, *r* (in Angstroms), of groups as discussed in the following: (a) Wells, P. R. In *Progress in Physical Organic Chemistry*; John Wiley & Sons, Inc.: New York, 1968; Vol. *6*, pp 111−145 and (b) Kagarise, R. E. *J. Am. Chem. Soc.* **1955**, *77*, 1377.

(27) Smith, M. B.; March, J. *March's Advanced Organic Chemistry: Reactions, Mechanisms, and Structure*, 5th ed.; John Wiley and Sons: New York, 2001; pp 20−36.

(28) Allen, F. H.; Kennard, O.; Watson, D. G.; Brammer, L.; Orpen, A. G.; Taylor, R. J. *J. Chem. Soc., Perkin Trans.* **1987**, *2*, S8.

(29) (a) Du Plessis, W. C.; Davis, W. L.; Cronje, S. J.; Swarts, J. C. *Inorg. Chim. Acta* **2001**, *314*, 97. (b) Von Chrzanowski, L. S.; Lutz, M.; Spek, A. L. *Acta Crystallogr.* **2006**, *E62*, m3318. (c) Von Chrzanowski, L. S.; Lutz, M.; Spek, A. L. *Acta Crystallogr.* **2007**, *C63*, m129.

(30) (a) Fleeting, K. A.; O'Brien, P.; Otway, D. J.; White, A. J. P.; Williams, D. J.; Jones, A. C. *Inorg. Chem.* **1999**, *38*, 1432. (b) Chmura, A. J.; Davidson, M. G.; Jones, M. D.; Lunn, M. D.; Mahon, M. F.; Johnson, A. J.; Kunchamchoo, P.; Roberts, S. L.; Wong, S. S. F. *Macromolecules* **2006**, *39*, 7250.

(31) Swarts, J. C.; Langner, E. H. G.; Krokeide-Hove, N.; Cook, M. J. *J. Mater. Chem.* **2001**, *11*, 434.

(32) (a) Swarts, J. C.; Nafady, A.; Roudebush, J. H.; Trupia, S.; Geiger, W. E. *Inorg. Chem.* **2009**, *48*, 2156. (b) Barriere, F.; Kirss, R. U.; Geiger, W. E. *Organometallics* **2005**, *24*, 48. (c) Barriere, F.; Camire, N.; Geiger, W. E.; Mueller-Westerhoff, U. T.; Sanders, R. *J. Am. Chem. Soc.* **2002**, *124*, 7262. (d) Kemp, K. C.; Fourie, E.; Conradie, J.; Swarts, J. C. *Organometallics* **2008**, *27*, 353. (e) Nafady, A.; Chin, T. T.; Geiger, W. E. *Organometallics* **2006**, *25*, 1654. (f) Chong, D. S.; Slote, J.; Geiger, W. E. *J. Electroanal. Chem.* **2009**, *630*, 28. (f) Barriere, F., F.; Geiger, W. E. *J. Am. Chem. Soc.* **2006**, *128*, 3980.

(33) Gericke, H. J.; Barnard, N. I.; Erasmus, E.; Swarts, J. C.; Cook, M. J.; Aquino, M. A. S. *Inorg. Chim. Acta* **2010**, *363*, 2222.

(34) (a) Evans, D. H.; O'Connell, K. M.; Peterson, R. A.; Kelly, M. J. *J. Chem. Educ.* **1983**, *60*, 290. (b) Kissinger, P. T.; Heineman, W. R. *J. Chem. Educ.* **1983**, *60*, 702. (c) Van Benschoten, J. J.; Lewis, J. Y.; Heineman, W. R. *J. Chem. Educ.* **1983**, *60*, 772. (d) Mobbott, G. A. J. *Chem. Educ.* **1983**, *60*, 697.

(35) (a) Cook, M. J.; Chambrier, I.; White, G. F.; Fourie, E.; Swarts, J. C. *Dalton Trans.* **2009**, 1136. (b) Fourie, E.; Swarts, J. C.; Chambrier, I.; Cook, M. J. *Dalton Trans.* **2009**, 1145.

(36) Chambrier, I.; Hughes, D. L.; Swarts, J. C.; Isare, B.; Cook, M. J. *Chem. Commun.* **2006**, 3504.

(37) LeSuer, R. J.; Buttolph, C.; Geiger, W. E. *Anal. Chem.* **2004**, *76*, 6395.

(38) Gericke, H. J.; Muller, A. J.; Swarts, J. C. *Inorg. Chem.* **2012**, *51*, 1552. (b) March, J. *Advanced Organic Chemistry*, 4th ed.; John Wiley and Sons: New York, 1992; pp 17−20, 263−269, 273−275.

(39) (a) Creutz, C., C.; Taube, H. J. *J. Am. Chem. Soc.* **1969**, *91*, 3988. (b) Geiger, W. E.; Van Order, N.; Pierce, D. T.; Bitterwolf, T. E.; Reingold, A. L.; Chasteen, N. D. *Organometallics* **1991**, *10*, 2403. (c) Van Order, N.; Geiger, W. E.; Bitterwolf, T. E.; Reingold, A. L. *J. Am. Chem. Soc.* **1987**, *109*, 5680. (d) Pierce, D. T.; Geiger, W. E. *Inorg. Chem.* **1994**, *33*, 373.

(40) (a) Karaoğlan, G. K.; Gümrükçü, G.; Koca, A.; Gül, A. *Dyes Pigm.* **2011**, *88*, 247. (b) Rawling, T.; McDonagh, A. M.; Colbran, S. B. *Inorg. Chim. Acta* **2008**, *361*, 49.

(41) Quinton, D.; Antunes, E.; Griveau, S.; Nyokong, T.; Bedioui, F. *Inorg. Chem. Commun.* **2011**, *14*, 330.

(42) Conradie, J.; Cameron, T. S.; Aquino, M. A. S.; Lamprecht, G. J.; Swarts, J. C. *Inorg. Chim. Acta* **2005**, *358*, 2530.

(43) Conradie, J.; Swarts, J. C. *Eur. J. Inorg. Chem.* **2011**, 2439.

(44) Auger, A.; Muller, A. J.; Swarts, J. C. *Dalton Trans.* **2007**, 3623.

(45) Erasmus, J. J. C.; Lamprecht, G. J.; Swarts, J. C.; Roodt, A.; Oskarsson, A. *Acta Crystallogr.* **1996**, *C52*, 3000.

(46) *CrysAlis CCD, Data Collection software*; Oxford Diffraction Ltd.: Wroclaw, Poland, 2005.

(47) *CrysAlis RED, Data Reduction program*; Oxford Diffraction Ltd.: Wroclaw, Poland, 2008; Issue 171.32.

(48) Sheldrick, G. M. *Acta Crystallogr.* **2008**, *A64*, 112−122.

(49) Brandenburg, K.; Putz, H. *DIAMOND*, Release 3.1a; Crystal Impact GbR: Bonn, Germany, 2005.